Published in final edited form as:
J Biomech. 2014 June 27; 47(9): 2055–2063. doi:10.1016/j.jbiomech.2013.10.058.

AN INVERSE MODELING APPROACH FOR STRESS ESTIMATION IN MITRAL VALVE ANTERIOR LEAFLET VALVULOPLASTY FOR IN-VIVO VALVULAR BIOMATERIAL ASSESSMENT

Chung-Hao Lee[1], **Rouzbeh Amini**[2], **Robert C. Gorman**[3], **Joseph H. Gorman III**[3], and **Michael S. Sacks**[1]

[1]Center for Cardiovascular Simulation Institute for Computational Engineering and Sciences (ICES) Department of Biomedical Engineering The University of Texas at Austin 201 East 24th Street, ACES 5.236 1 University Station C0200 Austin, TX 78712, USA

[2]Department of Biomedical Engineering The University of Akron Auburn Science and Engineering Center 275, West Tower Akron, OH 44325, USA

[3]Gorman Cardiovascular Research Group University of Pennsylvania 3400 Civic Center Blvd Philadelphia, PA 19104, USA

Abstract

Estimation of regional tissue stresses in the functioning heart valve remains an important goal in our understanding of normal valve function and in developing novel engineered tissue strategies for valvular repair and replacement. Methods to accurately estimate regional tissue stresses are thus needed for this purpose, and in particular to develop accurate, statistically informed means to validate computational models of valve function. Moreover, there exists no currently accepted method to evaluate engineered heart valve tissues and replacement heart valve biomaterials undergoing valvular stresses in blood contact. While we have utilized mitral valve anterior leaflet valvuloplasty as an experimental approach to address this limitation, robust computational techniques to estimate implant stresses are required. In the present study, we developed a novel numerical analysis approach for estimation of the in-vivo stresses of the central region of the mitral valve anterior leaflet (MVAL) delimited by a sonocrystal transducer array. The in-vivo material properties of the MVAL were simulated using an inverse FE modeling approach based on three pseudo-hyperelastic constitutive models: the neo-Hookean, exponential-type isotropic, and

For correspondence Michael S. Sacks, Ph.D. W. A. “Tex” Moncrief, Jr. Simulation-Based Engineering Science Chair I Director, Center for Cardiovascular Simulation Institute for Computational Engineering and Sciences Professor of Biomedical Engineering The University of Texas at Austin 201 East 24th St, Stop C0200 Austin, Texas 78712-1229.

Resubmitted to the Special Issue in the **Journal of Biomechanics** on Functional Tissue Engineering

Conflict of Interests
None of the authors have a conflict of interests with the present work.

full collagen-fiber mapped transversely isotropic models. A series of numerical replications with varying structural configurations were developed by incorporating measured statistical variations in MVAL local preferred fiber directions and fiber splay. These model replications were then used to investigate how known variations in the valve tissue microstructure influence the estimated ROI stresses and its variation at each time point during a cardiac cycle. Simulations were also able to include estimates of the variation in tissue stresses for an individual specimen dataset over the cardiac cycle. Of the three material models, the transversely anisotropic model produced the most accurate results, with ROI averaged stresses at the fully-loaded state of 432.6±46.5 kPa and 241.4±40.5 kPa in the radial and circumferential directions, respectively. We conclude that the present approach can provide robust instantaneous mean and variation estimates of tissue stresses of the central regions of the MVAL.

Keywords

In-vivo stress estimation; finite element (FE) inverse modeling; genetic algorithm; mapped collagen fiber architecture

1. Introduction

Today, almost 300,000 heart valve replacement surgeries are performed annually world-wide (Sacks and Schoen, 2002). However, durability of the bioprosthetic heart valve (BHV) continues to remain limited to the range of 10-15 years, and are often achieved only in patient with ages of 57 years or older (Schoen, 2005). In addition to complete valve replacement, valve repair has drawn gradually increasing attention for the treatment in patients, especially those with mitral valve (MR) diseases (Braunberger et al., 2001; Carpentier et al., 1980). Yet, recent long-term studies (Flameng et al., 2003; Flameng et al., 2008) showed that 10-15% of patients undergoes MV repair required re-operation for severe regurgitation within 10 years, and a 60% recurrence rate of significant MR in 3-5 years. Such failure mechanisms suggest that the repair-induced excessive tissue stresses and the resulting tissue damage are important factors (Accola et al., 2005; Fasol et al., 2004), which affect the MV interstitial cell metabolism and synthesis, tissue-level responses of the MV, and repair long-term durability.

Therefore, independent of design specifics, such as standard surgical prosthetic valve, percutaneous delivery, and engineered tissue-based valve, development of robust materials with improved durability and ability to account for post-natal somatic growth for pediatric applications remains an important clinical goal (Mol et al., 2009; Sacks et al., 2009b). Such development represents a unique cardiovascular engineering challenge resulting from the extreme valvular mechanical demands (Sacks et al., 2009a). Even basic methods to assess tissue-level stresses remain in development. Further, current valvular biomaterial assessment relies almost exclusively on device-level evaluations, which are confounded by simultaneous and highly coupled mechanical behaviors and fatigue, hemodynamics, and calcification. Thus, despite decades of clinical usage and growing popularity, there exists no acceptable method for assessing the intrinsic durability of valvular biomaterials.

Historically, the term “tissue engineering” is attributed to Y.C. Fung (Woo and Seguchi, 1989). The term underscored the importance of “the application of principles and methods of engineering and life sciences toward a fundamental understanding of the structure-function relationships in normal and pathologic mammalian tissues and the development of biological substitutes to restore, maintain, or improve tissue function.” Thus, it is imperative that fundamental structure-function understanding guides the reproduction of native tissue if it is to emulate its native counterpart successfully.

Clearly, the complex nature of native valvular tissue behavior (Sacks et al., 2009a) cannot be duplicated with simple, homogenous biomaterials assessed using conventional means. Consequently, to develop replacement valvular biomaterials we must more fully understand the fundamental mechanics of the native tissues and their potential replacement biomaterials as close as possible to the valvular physiological environment (Butler et al., 2000). In previous studies (Amini et al., 2012; Eckert et al., 2009; Rausch et al., 2011), in-vivo techniques were utilized to study in-vivo MV tissue strains under a variety of hemodynamic and pathological conditions. In particular, it was revealed that the center region of the MV anterior leaflet (MVAL) experienced substantially anisotropic stretches in the radial and circumferential directions during the cardiac cycle (Sacks et al., 2006a). This technique has also been employed in conjunction with a MVAL valvuloplasty model (Sacks et al., 2007) to assess the valvular stresses within a surgically implanted biomaterial. However, in this study a) only the strain at the center of the implant was used, b) no information on tissue microstructural variations was incorporated, and c) a homogeneous stress field was assumed. All of these effects will influence the resulting estimations of the tissue stresses.

When attempting to derive the local stress tensor of a valve leaflet utilizing in-vitro and in-vivo strain measurement techniques, the exact fiber microstructure and regional mechanical properties are required. These are in general not known on per-specimen/patient specific basis. Moreover, given the limited number of available markers in the in-vitro and in-vivo techniques, only low-order (e.g. linear or quadratic) estimates of the local deformation gradient tensor **F** within the region are feasible. Hence, development of an optimal method for accurately estimating a region of interest (ROI) stress tensor remains an open question. In addition, stress estimates of the complete MV have been conducted numerically from computational models (Einstein et al., 2004; Krishnamurthy et al., 2008; Krishnamurthy et al., 2009; Kunzelman et al., 1993a; Prot et al., 2010; Votta et al., 2008). However, many assumptions were made and thorough validation remain limited. Therefore, there is a need of such accurate in-vivo stress estimates, including both the mean stress tensor and its variation within a region for careful validation of the MV computational models in the development of novel replacement tissues.

In this work, we developed a numerical simulation method to estimate both the mean stress tensor and its variation within an ROI for the MVAL from existing in-vivo sonocrystal positional data. We also utilized our extensive knowledge of the MVAL microstructure to develop an estimate of the average stress variation due to the variations of collagen fiber microstructure. Our goal is to ultimately apply this systematic method for estimation of the repair-induced changes of the MV tissue stresses and provide guidelines for design of optimal surgical repair strategies with improved long-term durability.

2. Methods

2.1 Modeling framework and basic assumptions

The objective of this work is to estimate the regional tissue stresses of the MVAL based on in-vivo three-dimensional deformational data by utilizing a finite element (FE) modeling approach for stress analysis, in which an average structure of the MVAL was incorporated. In order to characterize the in-vivo mechanical properties of the MV constitutive models, an inverse FE modeling approach via the genetic algorithm was employed. The following assumptions were made in the numerical studies:

- The viscous and any related time-dependent effects were ignored and only the functional, quasi-elastic behaviors of the MV tissues were considered (Grashow et al., 2006a; Grashow et al., 2006b).
- MVAL tissue was modeled as a pseudo-hyperelastic material (Fung, 1993).
- The ROI was defined by the 2 by 2 sonocrystal marker array with an additional center marker (Figure 1-a).
- The local kinematics of the MVAL was represented by the prescribed in-vivo measured displacement data on the four edges.
- The FE simulation for stress analysis was carried from the reference configuration to the end of isovolumic relaxation (Figure 1-b), and the fully-loaded state was chosen for the statistical analysis of the MVAL regional stresses.

In this integrated modeling/experimental scenario, we sought to develop an estimate of the ROI stress tensor by averaging the stress at each point within the ROI. We noted that in developing our approach, variations in the resulting local tissue stresses can arise from the following sources within the ROI:

(1) Heterogeneities of the local deformation, resulting in $\mathbf{F}=\mathbf{F}(\mathbf{X},t)$, where $\mathbf{X}$ is the local position vector and t is time over the cardiac cycle.

(2) Variations in local tissue microstructure.

(3) Variations in local fiber mechanical properties.

The first two items can be directly quantified from experimental data: $\mathbf{F}$ can be determined at each point in the marker array by bilinear interpolation and tissue microstructure can be quantified using available experimental techniques, as we have done using small angle light scattering (SALS). It is the last item, the mechanical properties, which must be computed from the experimental data. Thus, we conducted a study to determine the average key fiber microstructural features from extant microstructural data on the MVAL. This key piece of information, when incorporated in the simulations, allowed us to quantify not only the mean ROI stress but also its variation from a single experimental run. This further allowed us to set confidence limits for the computed mean stresses from individual test specimens under a single set of experimental conditions.

2.2 In-vivo data acquisition

Three-dimensional echocardiography methodology for acquisition of the positional data was employed and the in-vivo sonocrystal data was acquired and utilized from the previous study (Amini et al., 2012). Briefly, nine male adult (30-45 kg) Dorsett sheep that have been raised for laboratory work by commercial vendors were used. The animals were induced with sodium thiopental (10-15 mg/kg IV), intubated, anesthetized, and ventilated with iso-fluorane (1.5-2%) and oxygen for transducer implantation, in compliance with the guidelines for human care (NIH Publication No. 85-23, revised 1985). With a sterile left lateral thoracotomy, a total number of five 2-mm hemispherical piezoelectric transducers were sutured on the MVAL, which defines the ROI for estimation of the in-vivo stresses (Figure 1-a), and the transducer wires were connected to a Sonometrices Series 5001 Digital Sonomicrometer (Sonometrics, London, Ontario). The sonomicrometry array localization (SAL) technique (Gorman et al., 1996) was then applied to determine the three-dimensional coordinates of each transducer at an acquisition interval of 5 ms as the transvalvular pressure was continuously monitored during cardiac cycles. The three-dimensional sonomicrometry positional data were taken following isoflurane titrated to achieve a systolic blood pressure of 90 mmHg. The 3D data were taken for fifteen cardiac cycles and the last cycle (Figure 1-b) was chosen as the representative since the cycle-to-cycle variations were typically very small. Followed by the previously developed approaches (Sacks et al., 2006a), the in-surface principal stretches of the MVAL were estimated based on the measurements using a single 5-node finite element (Figures 1-c, 2-b).

2.3 Statistical evaluation of the MVAL collagen fiber structure

Data from the previous studies of the MVAL fiber structure were used (Amini et al., 2012; He et al., 2005), where the SALS technique was utilized to determine the fiber angle dispersion function $\Gamma(\theta)$ (Sacks, 2003; Sacks et al., 1997). Since the laser beam diameter used for SALS measurement was 250 μm, a scanning grid of 250 μm by 250 μm was considered. At each data point, the preferred direction (PD) and orientation index were determined. For simplicity, we assumed the local $\Gamma(\theta)$ to be normally distributed with the mean fiber direction μ and standard deviation σ. The ROI mean and variance of μ and σ (μ_{PD},σ_{PD} and μ_{σ},σ_{σ}, respectively) were determined from the SALS data of *n=5* MVAL specimens using the methodology described in Appendix.

2.4 Mapping of collagen fiber structure

It should be noted that the fiber architecture measurements were performed for tissues in the excised, unloaded state. We have recently demonstrated that the MVAL is under substantial prestrain in-vivo compared to the excised, stress-free state (Amini et al., 2012). To account for the transformation between the excised and in-vivo reference states, the fiber dispersion distribution for the in-vivo MVAL was then determined by assuming an affine transformation (Billiar and Sacks, 1997) as follows

$$\Gamma(\beta) = \Gamma(\theta)\frac{\mathbf{N}(\theta)\cdot\mathbf{C}\mathbf{N}(\theta)}{J_{2d}} = \Gamma(\theta)\frac{\lambda_N^2}{J_{2d}} \quad (1)$$

where J_{2D} is the determinant of the in-plane deformation gradient tensor $\mathbf{F}_{2D}$, λ_N is the collagen fiber stretch ratio in the direction of $\mathbf{N}$, and $\mathbf{C}=(\mathbf{F}_{2D})^T\mathbf{F}_{2D}$ is the right Cauchy-Green deformation tensor. The OI value was then determined based on its definition associated with Γ(β), where β is the fiber angle in the deformed configuration computed using

$$\beta=tan^{-1}\left(\frac{F_{21}cos\theta+F_{22}sin\theta}{F_{11}cos\theta+F_{12}sin\theta}\right) \quad (2)$$

Once the fiber dispersion function Γ(β) was determined, the new values of μ and σ in the deformed configuration were directly computed.

Next, the preferred fiber direction measured at the excised state (Figure 2-a) was utilized to determine the local material axes $\hat{\mathbf{e}}_1$ and $\hat{\mathbf{e}}_2$ at the in-vivo reference configuration (Figure 2-b) through a single five-node element (Figure 2-c) by

$$\hat{\mathbf{e}}_1={}^1_0\mathbf{F}\cdot\begin{Bmatrix} cos\mu \\ sin\mu \\ 0 \end{Bmatrix} \text{ and } \hat{\mathbf{e}}_2={}^1_0\mathbf{F}\cdot\begin{Bmatrix} -sin\mu \\ cos\mu \\ 0 \end{Bmatrix} \quad (3)$$

where

$${}^1_0\mathbf{F}=\begin{bmatrix} \sum_{I=1}^{5} B_{xI}u_I & \sum_{I=1}^{5} B_{yI}u_I & s_x \\ \sum_{I=1}^{5} B_{xI}v_I & \sum_{I=1}^{5} B_{yI}v_I & s_y \\ \sum_{I=1}^{5} B_{xI}w_I & \sum_{I=1}^{5} B_{yI}w_I & s_z \end{bmatrix} \quad (4)$$

Herein, ${}^1_0\mathbf{F}$ is the deformation gradient between the excised (state 0) and in-vivo reference (state 1) configurations, $B_{xI}=\partial N_I/\partial x$ and $B_{yI}=\partial N_I/\partial y$ are the derivatives of the FE shape function N_I associated with marker I, $u_I=x_I-x_I'$, $v_I=y_I-y_I'$ and $w_I=z_I$ are the nodal displacements from the SALS grid plane to the physical domain, and $\mathbf{S}=[s_x,s_y,s_z]^T$ is the unit normal vector on the MVAL surface.

2.5 Generation of FE meshes with variations in local material axes and degrees of anisotropy

To investigate the effect of MVAL microstructure variations on the estimated ROI stresses, we generated a series of FE models by considering changes of the local material axes and degrees of material anisotropy for statistical analyses of the ROI averaged stress tensor and its variation based on numerical experiments. Briefly, for each element, the local preferred fiber direction was determined using standard statistical techniques for a normal distribution from the mean fiber direction and its variation (see Appendix), with element local material axes determined using Equations (3) and (4). Similarly, based on the same microstructural analyses, the degree of regional fiber alignment was determined, and this variation in material anisotropy was then incorporated into the collagen-fiber mapped constitutive model (Section 2.6). In the current study, five or more replicate geometries were generated for the

numerical experiments with the local preferred directions and standard deviations determined from their respective distributions (μ_{PD}, σ_{PD} and μ_{σ}, σ_{σ}).

2.6 Material models and inverse approach for parameter estimation

As discussed above, we considered the following constitutive models based on a pseudo-hyperelastic response (Fung, 1993) for describing the mechanical behaviors of the MVAL and for exploring the effects of the different forms of the constitutive model on the stress estimates. This was done with the following neo-Hookean model

$$\psi\left(\mathrm{I}_1\right)=\mathrm{C}_{10}\left(\mathrm{I}_1-3\right) \quad (5)$$

an exponential isotropic model with an neo-Hookean component

$$\psi\left(\mathrm{I}_1\right)=\mathrm{C}_{10}\left(\mathrm{I}_1-3\right)+\frac{\mathrm{c}_0}{2}\left\{\exp\left[\mathrm{c}_1\left(\mathrm{I}_1-3\right)^2\right]-1\right\} \quad (6)$$

and a full collagen-fiber mapped transversely isotropic model

$$\psi\left(\mathrm{I}_1,\mathrm{I}_4\right)=\mathrm{C}_{10}\left(\mathrm{I}_1-3\right)+\frac{\mathrm{c}_0}{2}\left\{\delta\exp\left[\mathrm{c}_1\left(\mathrm{I}_1-3\right)^2\right]+\left(1-\delta\right)\exp\left[\mathrm{c}_2\left(\mathrm{I}_4-1\right)^2\right]-1\right\} \quad (7)$$

For all three models, ψ is a strain energy density function, $I_1 = trace(\mathbf{C})$ and $I_4 = \mathbf{N}\cdot\mathbf{C}\cdot\mathbf{N}$ are the invariants, δ is a parameter governing the level of material anisotropy, and c_i are the material parameters quantified by the inverse approach. In this study, parameter δ was determined directly through a linear relationship with OI value using $\delta = OI(\sigma)/90°$ so that $\delta \in [0,1]$. Moreover, parameter C_{10} = 100 kPa was chosen, except for the neo-Hookean model, which accounts for the low-strain responses associated with the bending stiffness the valve tissues (Eckert et al., 2013).

We employed the following inverse modeling approach to characterize the in-vivo mechanical response for the MVAL. We utilized a global optimization technique (Figure 3), the genetic algorithm (Storn and Price, 1997), for finding an optimal set of material parameters $\mathbf{X}_{opt}$ which minimizes the error norm of displacement field between the in-vivo measurements and FE solutions:

$$\text{Objective function:}\quad \min_{\mathrm{x}} \mathrm{f}\left(\mathbf{x}\right)=\frac{1}{\mathrm{n}_{\mathrm{data}}}\sum_{\mathrm{i}=1}^{\mathrm{n}_{\mathrm{data}}}\left\|\mathbf{u}_{\mathrm{i}}^{\mathrm{in-vivo}}-\mathbf{u}_{\mathrm{i}}^{\mathrm{FEM}}\right\| \quad (8)$$

where n_{data}=40 is the number of time points of the 3D sonocrystal positional data from t_0 to t_5 during the cardiac cycle. Briefly, given a set of material parameters, an ABAQUS input file was generated for the simulation of the MVAL subjected to external pressure loading (Figure 1-b). The nodal displacements were obtained from the ABAQUS output file to construct the displacement vector, and the fitness function f(**x**) for each genome population was evaluated. The optimization process terminated when the change of the objective function is less than the set tolerance (TOL = 10^{-6}).

2.7 FE analyses of the ROI stresses

To analyze the stress field in the ROI, the MVAL surface was discretized into 40×40 thin-shell elements (to mimic the SALS measurement grid) with the characterized in-vivo constitutive models implemented in ABAQUS UMAT. Here, 1600 elements with equal element distances were constructed in the computational domain (Figure 2-c), and the isoparametric mapping was performed to obtain the FE discretized surface in the physical domain (Figure 2-b). The boundary nodes were prescribed with the displacement boundary conditions based on the five sonocrystal measured data using ABAQUS DISP; transvalvular pressures were applied on the element surfaces with ABAQUS AMPLITUDE; FE simulations of the MVAL during a cardiac cycle (t_0-t_5, see Figure 1-b) were performed, and stress output data were obtained using a python post processing script. The calculated stresses were averaged over the 1600 elements and regional variation of the stresses was estimated for each of the three constitutive models. Moreover, for each generated ROI configuration with different local material axes and degrees of material anisotropy, a FE simulation was carried out and the stress output was collected. The statistical analysis was then performed on the peak stresses using the results of the generated numerical replications.

3. Results

3.1 ROI fiber architecture and material parameter results

Collagen fiber directions mapped onto the MVAL surface, accounting for the transformation between the excised and in-vivo reference states, were in general very continuous with a fairly homogeneous strength of the fiber alignment within the region of interest (Table 1, Figures 4-a and 4-b), demonstrating the high fidelity of the mapping technique. For characterization of the material parameters in the inverse FE analysis, the objective function values at convergence were $\text{ObjFunc}^{\text{neo}} = 0.446$ mm, $\text{ObjFunc}^{\text{iso}} = 0.419$ mm, and $\text{ObjFunc}^{\text{mapped}} = 0.365$ mm for the three constitutive models (Table 2), respectively. Thus, the full collagen-fiber mapped transversely isotropic model (Eqn. 7) yielded the solution with minimum displacement errors relative to the in-vivo experimental data.

3.2 Estimated regional stress field

Stress-time profiles during a cardiac cycle predicted by using the three constitutive models were fairly regular in shape and smooth (Figures 5-a, 5-b, and 5-c), provided the anisotropic in-vivo stretches, with a similar pattern of rapid increasing followed by a plateau, in both radial and circumferential directions. Interesting, we also noted that the full collagen-fiber mapped transversely isotropic produces much smaller stresses estimates at the fully-loaded state (t_3), with substantially larger stresses in the radial direction ranging from 380 to 480 kPa and the circumferential stresses ranging from 200 to 280 kPa given the radial stretch of 32% and circumferential stretch of 11%, whereas ~28% and ~11% higher of the estimated ROI stress values were reported for the neo-Hookean and exponential-type isotropic models (Table 3, Figures 6-a, 6-b, and 6-c).

3.3 Effect of variations in local fiber directions and degrees of anisotropy on ROI stresses

The predicted ROI peak stresses at the fully-loaded state (t_3) were ~520 and ~285 kPa for the radial and circumferential components, respectively, for the numerical experiments with variations in the local fiber directions, whereas the peak stress components of ~600 and ~280 kPa in the radial and circumferential directions were reported by considering variations in both the local fiber directions and degrees of material anisotropy (Figure 7 and Table 4). The resulting radial stress variations in the latter case are expectedly larger (by ~5%) than the former situation (~2.4%) due to introducing additional fiber microstructural. However, this additional variation led to very small deviations of the estimated peak circumferential stress component.

4. Discussion

4.1 Overall observations and comparisons to existing results

In the present study, we developed a numerical approach for systematic estimation of the in-vivo stresses of a region of interest within the normal functioning MVAL, delimited by a sonocrystal transducer array, based on the 3D positional data. The in-vivo mechanical properties of the MVAL were simulated using an inverse FE modeling approach based on a pseudo-hyperelasticity formulation. Interestingly, the fiber mapped anisotropic model (Eqn. 7) produced both the lowest ROI averaged stresses and optimal objective function value among the three constitutive models considered. This result indicates that this constitutive model form is more appropriate for describing the in-vivo MVAL mechanical behavior.

While direct comparison to related work is not possible, we note that Krishnamurthy et al. (Krishnamurthy et al., 2009) presented the results of stress estimates t_{CC} = 1,540±838 kPa and t_{RR} = 1,513±826 kPa (reported as the average±SEM determined from nine separate ovine specimens) at transvalvular pressures of 60-70 mmHg. In this study marker videofluoroscopy and an inverse FE analysis were also used. However, the obtained stress values are higher than our estimations, potentially due to the linear elastic material adopted in their study. Moreover, fairly isotropic behaviors of the MV tissue stresses were observed in their work although an orthotropic material was considered. On the other hand, our results agreed qualitatively with the anisotropic MV tissue behaviors previously reported (Grashow et al., 2006b). We noted too that others (Prot, 2007; Rausch et al., 2011; Rausch et al., 2012) also performed similar constitutive model form studies for the MV leaflet tissues. The main novelty of the present approach is our incorporation of statistical structural information of the MVAL ROI to determine not only the mean stress tensor, but also its variation within the ROI for an individual ovine specimen. This approach can greatly aid investigations of how the variations and time changes in the fiber structure and fiber mechanical properties influence the estimated ROI stresses over the cardiac cycle. For example, our approach can be used in valvuloplasty model studies of time-evolving changes in the material subjected to valvular stresses in blood contract using available sonocrystal data. Moreover, our approach is quite general which can be used in assisting the development of specialized engineered tissues or related biomaterials for replacement heart valves

4.2 Use of novel surgical and computational modeling in valve model validation and in the development of novel heart valve replacement tissues

BHV durability continues to remain limited to the range of 10-15 years; often achieved only in patient ages 57 years or older (Schoen, 2005). While there are several critical aspects responsible for this lack of progress, a major reason is that there is no existing model (in-vitro bench-top, large animal, or computational) to evaluate and predict in-vivo replacement valvular tissue performance between rat subdermal implantation, which provides no mechanical stress and blood interactions, and full heart valve replacement, where device design related failure is common factor. Thus, regardless of the design specifics, the lack of rigorous, mechanistic knowledge of in-vivo durability and means to simulate tissue responses in new valve designs have lead, in large part, to the current stagnation in valve replacement development (Schoen and Levy, 2005).

As in many medical device fields, continued progress requires a much more sophisticated level of understanding, especially at the component material level. Moreover, in conjunction with bench top and large animal experimental studies, computational simulations can help in defining how evolving biomaterial biomechanical properties drive valvular function and performance. Such approaches have been recently promoted at the FDA/NHLBI/NSF workshop on “Computer Methods for Cardiovascular Devices” held on June 10-11, 2010, Rockville, MD (FDA/NHLBI/NSF). A consensus at this meeting was that we are now entering a level of bioengineering knowledge and ability wherein computational approaches can be realistically applied to cardiovascular devices, as anticipated by our group in 2006 (Sacks et al., 2006b).

The proposed approach represents a logical step in models that incorporate collagen architecture, accurate material models, and highly accurate valvular kinematics (Lee et al., 2013). This approach is consistent, for example, with the hypothesis that MV tissue failure results from abnormally excessive stresses (from disease or improper repair). Thus, truly predictive valvular FE modeling cannot proceed without accurate experimentally-derived constitutive models (Sun et al., 2005). The present study is a step towards developing such models directly based on extensive in-vivo and in-vitro studies (Grashow et al., 2006a; Grashow et al., 2006b; Sacks and Yoganathan, 2008; Stella and Sacks, 2007).

4.3 Study limitations

Since we measured the surface strains of the MVAL as well as in-plane stress calculation, we implicitly neglected the variations due to leaflet thickness. The MV leaflets are composed of four layers: atrialis, spongiosa, fibrosa, and ventricularis (Kunzelman et al., 1993b). We assumed that the relative motions between different layers, if any, had negligible effects on the measured deformation in the midsection of the MVAL and the non-uniform mechanical properties thorough different layers were reasonably represented by a bulk constitutive model. Recent results for the aortic heart valve has indicated that the leaflet layers are tightly bonded and do not exhibit sliding during bending (Buchanan and Sacks, in-press), supporting this assumption. Finally, we note that the stress and strain fields were obtained only for the midsection of the MV anterior leaflet, since this is focus of the present study. However, in principal this method can be applied at other regions of the MVAL in

future studies. Given the high reproducibility of the measurements and the computational modeling framework, we believe that this is a reasonable approach applicable for MV leaflet tissues under surgical repair conditions.

4.4 Summary

In this study, we demonstrated a numerical analysis approach for estimation of the in-vivo stresses of a region of interest, delimited by the sonocrystal transducer array, within the normal functioning MVAL based on the 3D positional data. Estimated ROI averaged stresses at the fully-loaded state were 432.6±46.5 kPa and 241.4±40.5 kPa in the radial and circumferential directions. The in-vivo material properties of the MVAL were also characterized using an inverse FE modeling approach based on the hyperelasticity formulation. A series of numerical replications with various ROI configurations considering variations in the local fiber directions and degrees of material anisotropy were generated based upon the measured collagen fiber microstructural information to investigate how these variations in microstructures influence the estimated ROI stresses and to demonstrate the robustness and reliability of the computational framework for in-vivo stress estimation.

Acknowledgments

This work was funded by the funding from the NIH grants R01 HL119297, HL108330, HL63954, HL103723, HL73021, and F32 HL110651. Dr. C.H. Lee was supported in part by an ICES Postdoctoral Fellowship.

Appendix

To compute the average collagen-fiber microstructural architecture, we used the following regional averaging technology. In particular, the complex angle at each location associated with the main fiber direction ’s and its mean were computed by

$$\mathrm{v_p}=\exp\left[2\mathrm{i}\varphi_\mathrm{p}\right],\ \text{and}\ \ \bar{\mathrm{v}}=\frac{1}{\mathrm{n}}\sum_{\mathrm{p}=1}^{\mathrm{n}}\mathrm{v_p}=\frac{1}{\mathrm{n}}\sum_{\mathrm{p}=1}^{\mathrm{n}}\exp\left[2\mathrm{i}\varphi_\mathrm{p}\right] \quad (9)$$

The averaged preferred fiber direction was then calculated by

$$\mu_{\mathrm{PD}}=\begin{cases}\frac{1}{2}tan^{-1}\left(\frac{\mathrm{lm}\left(\bar{\mathrm{v}}\right)}{\mathrm{Re}\left(\bar{\mathrm{v}}\right)}\right)-\frac{\pi}{2}, & tan^{-1}\left(\frac{\mathrm{lm}\left(\bar{\mathrm{v}}\right)}{\mathrm{Re}\left(\bar{\mathrm{v}}\right)}\right)>0\\ \frac{1}{2}tan^{-1}\left(\frac{\mathrm{lm}\left(\bar{\mathrm{v}}\right)}{\mathrm{Re}\left(\bar{\mathrm{v}}\right)}\right)+\frac{\pi}{2}, & tan^{-1}\left(\frac{\mathrm{lm}\left(\bar{\mathrm{v}}\right)}{\mathrm{Re}\left(\bar{\mathrm{v}}\right)}\right)<0\end{cases} \quad (10)$$

where $lm\left(\bar{\mathrm{v}}\right)$ and $Re\left(\bar{v}\right)$ are the imaginary and real parts of $\bar{v}$. Moreover, the average distribution function was defined by

$$\bar{\Gamma}\left(\theta\right)=\frac{1}{\mathrm{n}}\sum_{\mathrm{p}=1}^{\mathrm{n}}\Gamma_\mathrm{p}\left(\theta\right) \quad (11)$$

where the standared deviation σ_{PD} can be computed accordingly.

References

Accola KD, Scott ML, Thompson PA, Palmer GJ 3rd, Sand ME, Ebra G. Midterm outcomes using the physio ring in mitral valve reconstruction: experience in 492 patients. Ann Thorac Surg. 2005; 79:1276–1283. discussion 1276-1283. [PubMed: 15797062]

Amini R, Eckert CE, Koomalsingh K, McGarvey J, Minakawa M, Gorman JH, Gorman RC, Sacks MS. On the in vivo deformation of the mitral valve anterior leaflet: effects of annular geometry and referential configuration. Ann Biomed Eng. 2012; 40:1455–1467. [PubMed: 22327292]

Billiar KL, Sacks MS. A method to quantify the fiber kinematics of planar tissues under biaxial stretch. J Biomech. 1997; 30:753–756. [PubMed: 9239558]

Braunberger E, Deloche A, Berrebi A, Abdallah F, Celestin JA, Meimoun P, Chatellier G, Chauvaud S, Fabiani JN, Carpentier A. Very long-term results (more than 20 years) of valve repair with carpentier's techniques in nonrheumatic mitral valve insufficiency. Circulation. 2001; 104:I8–11. [PubMed: 11568021]

Buchanan, RM.; Sacks, MS. Interlayer micromechanics of the aortic heart valve leaflet. Biomech Model Mechanobiol. in-press

Butler DL, Goldstein SA, Guilak F. Functional tissue engineering: the role of biomechanics. J Biomech Eng. 2000; 122:570–575. [PubMed: 11192376]

Carpentier A, Chauvaud S, Fabiani JN, Deloche A, Relland J, Lessana A, D'Allaines C, Blondeau P, Piwnica A, Dubost C. Reconstructive surgery of mitral valve incompetence: ten-year appraisal. J Thorac Cardiovasc Surg. 1980; 79:338–348. [PubMed: 7354634]

Eckert CE, Fan R, Mikulis B, Barron M, Carruthers CA, Friebe VM, Vyavahare NR, Sacks MS. On the biomechanical role of glycosaminoglycans in the aortic heart valve leaflet. Acta Biomaterialia. 2013; 9:4653–4660. [PubMed: 23036945]

Eckert CE, Zubiate B, Vergnat M, Gorman JH 3rd, Gorman RC, Sacks MS. In vivo dynamic deformation of the mitral valve annulus. Ann Biomed Eng. 2009; 37:1757–1771. [PubMed: 19585241]

Einstein DR, Kunzelman KS, Reinhall PG, Cochran RP, Nicosia MA. Haemodynamic determinants of the mitral valve closure sound: a finite element study. Med Biol Eng Comput. 2004; 42:832–846. [PubMed: 15587476]

Fasol R, Meinhart J, Deutsch M, Binder T. Mitral valve repair with the Colvin Galloway Future Band. Ann Thorac Surg. 2004; 1988; 77:1985–1988. [PubMed: 15172250]

FDA/NHLBI/NSF, Workshop on "Computer Methods for Cardiovascular Devices

Flameng W, Herijgers P, Bogaerts K. Recurrence of mitral valve regurgitation after mitral valve repair in degenerative valve disease. Circulation. 2003; 107:1609–1613. [PubMed: 12668494]

Flameng W, Meuris B, Herijgers P, Herregods M-C. Durability of mitral valve repair in Barlow disease versus fibroelastic deficiency. The Journal of thoracic and cardiovascular surgery. 2008; 135:274–282. [PubMed: 18242250]

Fung, YC. Biomechanics: Mechanical Properties of Living Tissues. 2nd. Springer Verlag; New York: 1993.

Gorman JH 3rd, Gupta KB, Streicher JT, Gorman RC, Jackson BM, Ratcliffe MB, Bogen DK, Edmunds LH Jr. Dynamic three-dimensional imaging of the mitral valve and left ventricle by rapid sonomicrometry array localization. J Thorac Cardiovasc Surg. 1996; 112:712–726. [PubMed: 8800160]

Grashow JS, Sacks MS, Liao J, Yoganathan AP. Planar biaxial creep and stress relaxation of the mitral valve anterior leaflet. Ann Biomed Eng. 2006a; 34:1509–1518. [PubMed: 17016761]

Grashow JS, Yoganathan AP, Sacks MS. Biaixal stress-stretch behavior of the mitral valve anterior leaflet at physiologic strain rates. Ann Biomed Eng. 2006b; 34:315–325. [PubMed: 16450193]

He Z, Ritchie J, Grashow JS, Sacks MS, Yoganathan AP. In vitro dynamic strain behavior of the mitral valve posterior leaflet. J Biomech Eng. 2005; 127:504–511. [PubMed: 16060357]

Krishnamurthy G, Ennis DB, Itoh A, Bothe W, Swanson JC, Karlsson M, Kuhl E, Miller DC, Ingels NB Jr. Material properties of the ovine mitral valve anterior leaflet in vivo from inverse finite element analysis. Am J Physiol Heart Circ Physiol. 2008; 295:H1141–H1149. [PubMed: 18621858]

Krishnamurthy G, Itoh A, Bothe W, Swanson JC, Kuhl E, Karlsson M, Craig Miller D, Ingels NB Jr. Stress-strain behavior of mitral valve leaflets in the beating ovine heart. J Biomech. 2009; 42:1909–1916. [PubMed: 19535081]

Kunzelman KS, Cochran RP, Chuong C, Ring WS, Verrier ED, Eberhart RD. Finite element analysis of the mitral valve. J Heart Valve Dis. 1993a; 2:326–340.

Kunzelman KS, Cochran RP, Murphree SS, Ring WS, Verrier ED, Eberhart RC. Differential collagen distribution in the mitral valve and its influence on biomechanical behaviour. J Heart Valve Dis. 1993b; 2:236–244. [PubMed: 8261162]

Lee, C-H.; Oomen, PA.; Rabbah, J.; Yoganathan, A.; Gorman, R.; Gorman, J.; Amini, R.; Sacks, M. A High-Fidelity and Micro-anatomically Accurate 3D Finite Element Model for Simulations of Functional Mitral Valve. In: Ourselin, S.; Rueckert, D.; Smith, N., editors. Functional Imaging and Modeling of the Heart. Springer; Berlin Heidelberg: 2013. p. 416-424.

Mol A, Smits AI, Bouten CV, Baaijens FP. Tissue engineering of heart valves: advances and current challenges. Expert Rev Med Devices. 2009; 6:259–275. [PubMed: 19419284]

Prot V, Skallerud B, Sommer G, Holzapfel GA. On modelling and analysis of healthy and pathological human mitral valves: two case studies. Journal of the mechanical behavior of biomedical materials. 2010; 3:167–177. [PubMed: 20129416]

Rausch MK, Bothe W, Kvitting JP, Goktepe S, Miller DC, Kuhl E. In vivo dynamic strains of the ovine anterior mitral valve leaflet. Journal of Biomechanics. 2011; 44:1149–1157. [PubMed: 21306716]

Sacks MS. Incorporation of experimentally-derived fiber orientation into a structural constitutive model for planar collagenous tissues. J Biomech Eng. 2003; 125:280–287. [PubMed: 12751291]

Sacks MS, David Merryman W, Schmidt DE. On the biomechanics of heart valve function. J Biomech. 2009a; 42:1804–1824. [PubMed: 19540499]

Sacks MS, Enomoto Y, Graybill JR, Merryman WD, Zeeshan A, Yoganathan AP, Levy RJ, Gorman RC, Gorman JH 3rd. In-vivo dynamic deformation of the mitral valve anterior leaflet. Ann Thorac Surg. 2006a; 82:1369–1377. [PubMed: 16996935]

Sacks MS, Hamamoto H, Connolly JM, Gorman RC, Gorman JH 3rd, Levy RJ. In vivo biomechanical assessment of triglycidylamine crosslinked pericardium. Biomaterials. 2007; 28:5390–5398. [PubMed: 17822757]

Sacks MS, Mirnajafi A, Sun W, Schmidt P. Bioprosthetic heart valve heterograft biomaterials: structure, mechanical behavior and computational simulation. Expert Rev Med Devices. 2006b; 3:817–834. [PubMed: 17280546]

Sacks MS, Schoen FJ. Collagen fiber disruption occurs independent of calcification in clinically explanted bioprosthetic heart valves. J Biomed Mater Res. 2002; 62:359–371. [PubMed: 12209921]

Sacks MS, Schoen FJ, Mayer JE. Bioengineering challenges for heart valve tissue engineering. Annu Rev Biomed Eng. 2009b; 11:289–313. [PubMed: 19413511]

Sacks MS, Smith DB, Hiester ED. A small angle light scattering device for planar connective tissue microstructural analysis. Ann Biomed Eng. 1997; 25:678–689. [PubMed: 9236980]

Sacks MS, Yoganathan AP. Heart valve function: a biomechanical perspective. Philos Trans R Soc Lond B Biol Sci. 2008; 363:2481.

Schoen FJ. Cardiac valves and valvular pathology: update on function, disease, repair, and replacement. Cardiovasc Pathol. 2005; 14:189–194. [PubMed: 16009317]

Schoen FJ, Levy RJ. Calcification of tissue heart valve substitutes: progress toward understanding and prevention. Ann Thorac Surg. 2005; 79:1072–1080. [PubMed: 15734452]

Stella JA, Sacks MS. On the biaxial mechanical properties of the layers of the aortic valve leaflet. J Biomech Eng. 2007; 129:757–766. [PubMed: 17887902]

Storn R, Price K. Differential evolution - A simple and efficient heuristic for global optimization over continuous spaces. J Global Optim. 1997; 11:341–359.

Sun W, Abad A, Sacks MS. Simulated bioprosthetic heart valve deformation under quasi-static loading. Journal of Biomechanial Engineering. 2005; 127:905–914.

Votta E, Caiani E, Veronesi F, Soncini M, Montevecchi FM, Redaelli A. Mitral valve finite-element modelling from ultrasound data: a pilot study for a new approach to understand mitral function and clinical scenarios. Philos Transact A Math Phys Eng Sci. 2008; 366:3411–3434.

Woo, SLY.; Seguchi, Y. Tissue Engineering - 1989. Asme; New York: 1989. BED ed

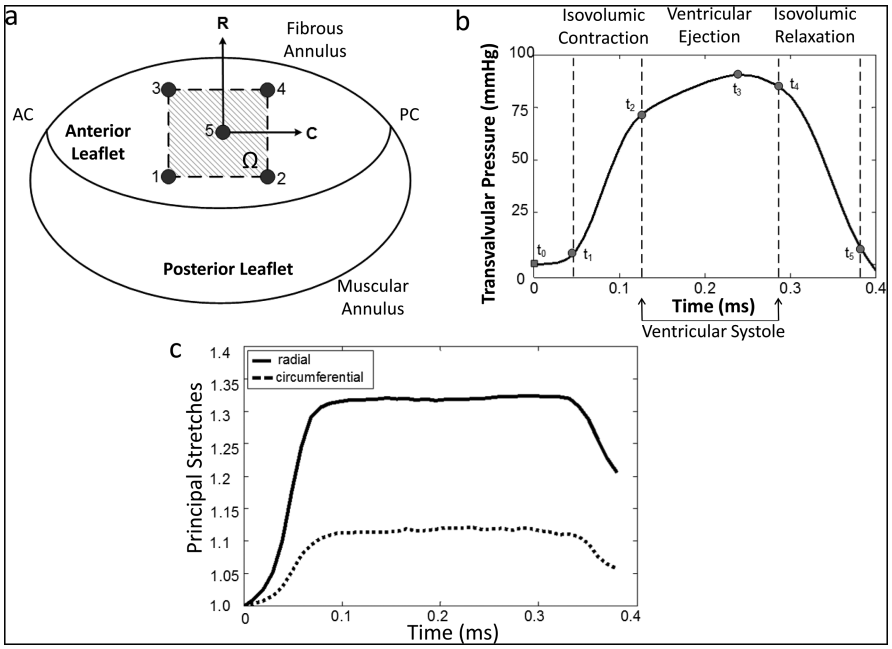

Figure 1.

Schematic of the ovine mitral valve anterior and posterior leaflets and the sonocrystal array for in-vivo measurements, (b) illustration of a typical cardiac cycle with specific time points, and (c) in-vivo measured principal stretches in the radial and circumferential directions.

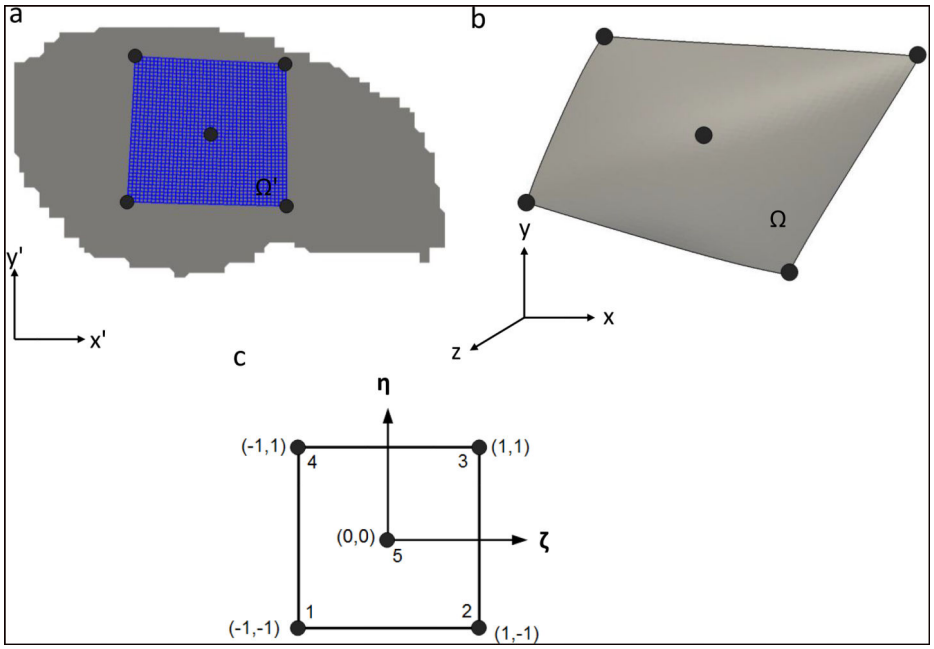

Figure 2.

Schematic diagram showing the mapping of the MV anterior leaflet between the SALS data coordinates Ω' and the physical domain Ω: (a) Sonocrystal markers and 40×40 elements reconstructed on the SALS data coordinates (x',y') associated with the flatten MV anterior leaflet tissues in grey, and (b) the fitting surface of the anterior leaflet using 5 sonocrystal markers at the physical coordinates (x,y,z), through the computational domain (ξ,η) with a 5-node finite element as illustrated in (c).

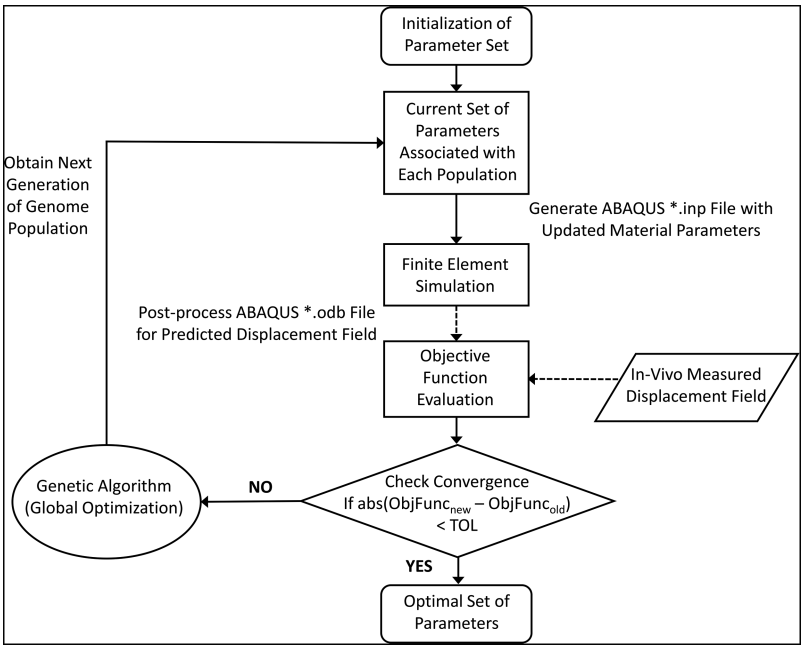

Figure 3.

Flowchart of an inverse modeling approach via the genetic algorithm for characterization of the material parameters of the constitutive model for the MVAL tissues.

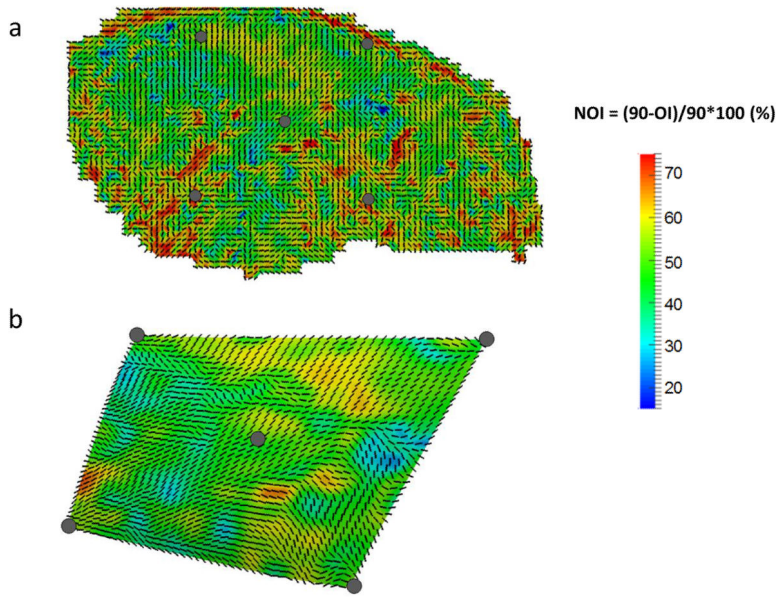

Figure 4.

(a) Measured collagen fiber architecture (preferred fiber directions in black dashes and strengths of fiber alignment in different colors) of the MV anterior leaflet via the SALS technique with 5 sonocrystal markers, (b) mapped collagen fiber architecture onto the 3D MVAL surface considering the mapping from the excised stress-free configuration to the in-vivo reference state.

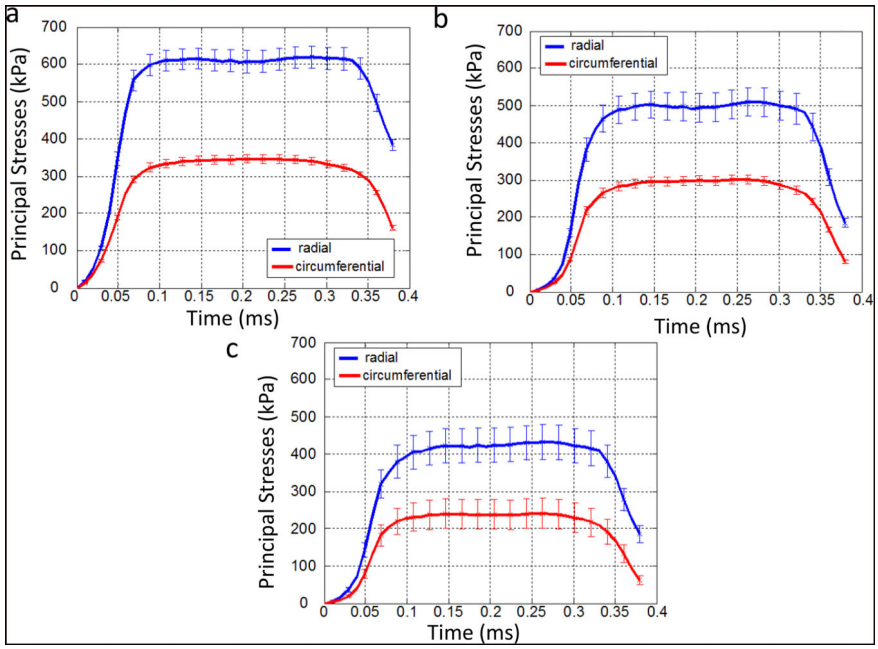

Figure 5.

Estimated mean principal stresses and the variation ($t_{RR,CC} \pm SD_{t_{RR,CC}}$) over the region of interest (Ω) in the radial and circumferential directions from t_0 to t_5: (a) neo-Hookean material, (b) exponential-type isotropic material, and (d) full collagen-fiber mapped transversely isotropic material.

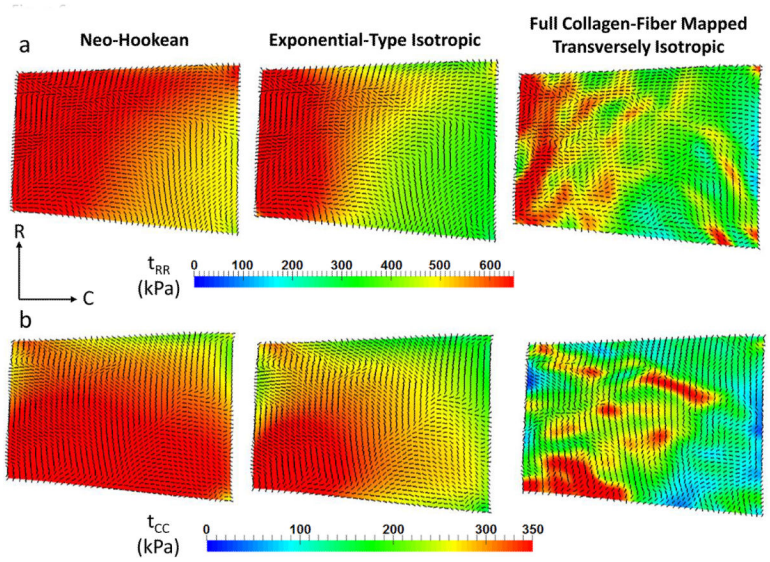

Figure 6.

FE predicted principal stresses and directions of the MVAL at the fully-loaded state (t_3) by using the three constitutive models: (a) the radial direction and (b) the circumferential direction.

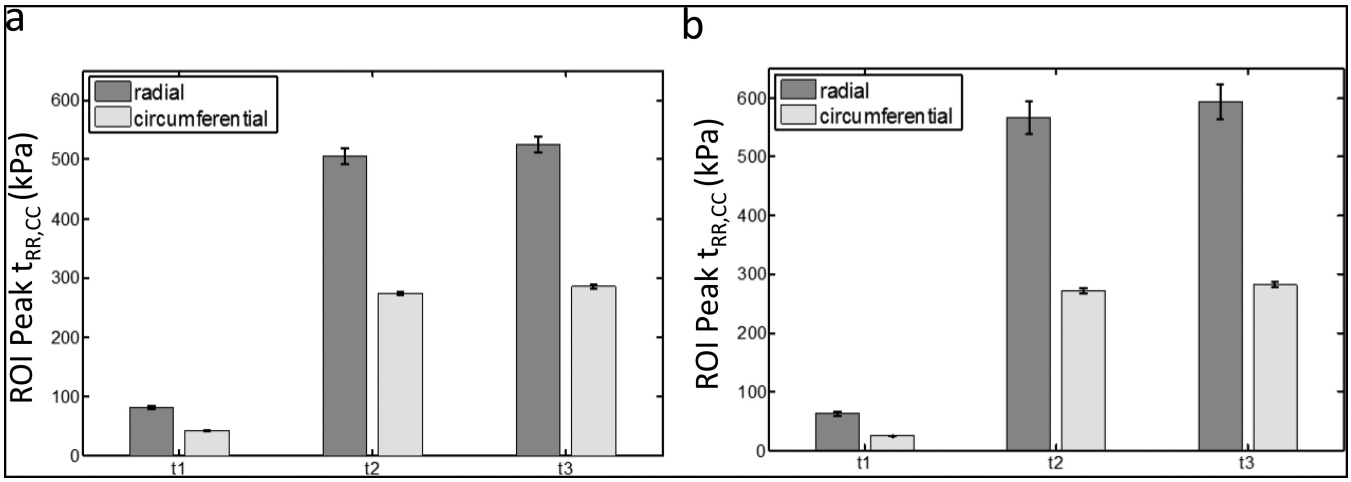

Figure 7.

Estimated ROI peak principal stresses and associated sample variations (n = 10) in the radial and circumferential directions at various time instants (t_1, t_2, t_3) considering: (a) variation in the local fiber directions, and (b) variations in both the local fiber directions and degrees of material anisotropy.

Table 1

Summary of the results of the ROI MVAL fiber architecture based on the statistical analysis

	μ_{PD} (deg.)	σ_{PD} (deg.)	μ_{σ} (deg.)	σ_{σ} (deg.)
Excised state (SALS scanning)	72.24	42.58	36.85	5.47
In-vivo reference state (mapped, Eqn. (1)-(4))	70.76	38.93	44.06	10.36

Table 2

Characterized in-vivo material parameters for various constitutive models of the MV anterior leaflet via the inverse modeling approach

Neo-Hookean model, Eqn. (5)	C_{10} (MPa)			
	0.3367			
Exponential-type isotropic model, Eqn. (6)	C_{10} (MPa)	c_0 (MPa)	c_1	
	0.1	2.9684	0.2661	
Full collagen-fiber mapped transversely isotropic model, Eqn. (7)	C_{10} (MPa)	c_0 (MPa)	c_1	c_2
	0.1	2.8351	0.4252	0.4316

C_{10} is chosen for the low-strain responses and for numerical stability as implemented in ABAQUS UMAT.

A mean value of 44.06° for the standard deviation of the fiber angular distributions is considered for characterization of other material parameters, which results in δ=0.4231.

Table 3

Estimation of the ROI averaged stresses at the fully-loaded state for three constitutive models

Model type	t_{CC} **(kPa)**	t_{RR} **(kPa)**
Neo-Hookean model, Eqn. (5)	344.3 ± 11.5	617.9 ± 28.6
Exponential-type isotropic model, Eqn. (6)	301.4 ± 12.2	509.5 ± 38.4
Full collagen-fiber mapped transversely isotropic model, Eqn. (7)	241.4 ± 40.5	432.6 ± 46.5

Table 4

Estimation of the ROI peak stresses using 10 numerical replications by considering variations in the local fiber directions and degrees of material anisotropy at time points t_1-t_3 of the cardiac cycle (see Fig. 4).

		t_{CC} (kPa)	t_{RR} (kPa)
Variations in the local fiber directions	t_1	42.2 ± 1.16	80.9 ± 2.21
	t_2	273.8 ± 3.21	505.7 ± 13.3
	t_3	285.1 ± 3.28	525.2 ± 14.1
Variations in both the local fiber directions and degrees of material anisotropy	t_1	24.8 ± 0.27	62.3 ± 3.59
	t_2	270.8 ± 4.81	566.4 ± 28.1
	t_3	281.9 ± 4.76	593.2 ± 29.6